

Identifying new high-confidence polluted white dwarf candidates using Gaia XP spectra and Self-Organizing Maps

XABIER PÉREZ-COUTO ^{1,2} LARA PALLAS-QUINTELA ^{1,2} MINIA MANTEIGA ^{3,2} EVA VILLAVER ^{4,5} AND
CARLOS DAFONTE ^{1,2}

¹*Universidade da Coruña (UDC), Department of Computer Science and Information Technologies,
Campus de Elviña s/n, 15071, A Coruña, Galiza, Spain*

²*CIGUS CITIC, Centre for Information and Communications Technologies Research,
Universidade da Coruña, Campus de Elviña s/n, 15071 A Coruña, Galiza, Spain*

³*Universidade da Coruña (UDC), Department of Nautical Sciences and Marine Engineering,
Paseo de Ronda 51, 15011, A Coruña, Galiza, Spain*

⁴*Instituto de Astrofísica de Canarias, 38200 La Laguna, Tenerife, Spain*

⁵*Universidad de La Laguna (ULL), Astrophysics Department,
38206 La Laguna, Tenerife, Spain*

(Received July 26, 2024; Accepted October 18, 2024)

ABSTRACT

The identification of new white dwarfs (WDs) polluted with heavy elements is important since they provide a valuable tool for inferring chemical properties of putative planetary systems accreting material on their surfaces. The Gaia space mission has provided us with an unprecedented amount of astrometric, photometric, and low resolution (XP) spectroscopic data for millions of newly discovered stellar sources, among them thousands of WDs. In order to find WDs among this data and to identify which ones have metals in their atmospheres, we propose a methodology based on an unsupervised artificial intelligence technique called Self-Organizing Maps (SOM). In our approach a nonlinear high-dimensional dataset is projected on a 2D grid map where similar elements fall into the same neuron.

By applying this method, we obtained a clean sample of 66,337 WDs. We performed an automatic spectral classification analysis to them, obtaining 143 bona fide polluted WD candidates not previously classified in the literature. The majority of them are cool WDs and we identify in their XP spectra several metallic lines such as Ca, Mg, Na, Li, and K. The fact that we obtain similar precision metrics than those achieved with recent supervised techniques highlights the power of our unsupervised approach to mine the Gaia archives for hidden treasures to follow-up spectroscopically with higher resolution.

Keywords: white dwarfs — methods: data analysis — catalogs

1. INTRODUCTION

White dwarfs (WD) are the degenerate stellar remnants of low- to intermediate- mass stars ($\leq 8M_{\odot}$) (Iben et al. 1997). Due to their high density ($\sim 10^3$ kg/m³), WDs have fully stratified interiors, containing a degenerate core composed of carbon and oxygen. This core is encased in a thin helium mantle, which constitutes at most about 1% of the white dwarf’s mass. Surrounding this helium layer is an even thinner but opaque hydrogen envelope, which makes up no more than approximately 0.01% of the mass. In some cases, Carbon can also be detected in the atmosphere, diffused upwards from the

nuclei by a convection zone under the Helium layer (Pelletier et al. 1986).

More exciting are those WDs that show heavy metal lines in their atmospheres. In cool WDs (below approximately 25,000 K), heavy elements tend to diffuse downward in the atmospheres due to gravitational settling in the presence of strong gravitational fields (Koester 2009). Since the diffusion timescales due to gravitational settling are much shorter than the evolutionary time scales of WDs, those metals cannot be primordial; they must have been accreted, with the accretion of rocky material from planetesimals being the most widely accepted explanation (Koester & Wilken 2006; Zucker-

man et al. 2007; Farihi et al. 2010; Veras et al. 2024). For this reason, the detection of those polluted WDs is nowadays an effervescent field and a valuable tool to infer the presence and physical properties of exoplanets (Mustill et al. 2018; Izquierdo et al. 2020; Maldonado et al. 2020, 2021; Klein et al. 2021; Trierweiler et al. 2023; Swan et al. 2023; Xu et al. 2024).

WD cooling tracks start at high temperatures ($\sim 10^5 K$) and thus they are located in the blue part of the color-magnitude diagram (CMD). The low luminosity resulting from their small radius (approximately 10,000 km) (Carvalho et al. 2016) makes WDs very difficult to observe. In fact, as of 2018, only about 30,000 WDs had been identified. Fortunately, the Gaia mission has changed the rules of the game by providing $G_{BP} - G_{RP}$ colors from Blue (BP) and Red (RP) photometers, as well as parallaxes and full astrometry, for 1460 million sources in the Gaia Data Release 3 (Gaia DR3) (Gaia Collaboration 2023). Gaia low resolution BP/RP (XP) mean spectra are also provided for ~ 220 million sources by using spectrophotometry (Carrasco et al. 2021).

Since classifying such a large number of spectra by human visual inspection is not feasible, several works took advantage of supervised machine learning techniques to train algorithms with labeled WD spectra and, subsequently, to predict the spectral classes of the rest of unlabeled objects. In Vincent et al. (2023) and Vincent et al. (2024) a neural network was trained with $\sim 14,000$ Sloan Digital Sky Survey (SDSS) WDs in order to predict if a Gentile-Fusillo et al. (2021) (hereafter, GF+21) source is a WD or a contaminant. Subsequently, the sources are classified in one of the primary spectral classes: DA (H - rich), DB (He I - rich), DO (He II - rich), DQ (C - rich), DZ (metal - rich) or DC (featureless) WDs, (Sion et al. 1983) with precisions above 90% for DA, DB, and DO types, but lower for DC, DQ, and DZ. García-Zamora et al. (2023) used the Random Forest algorithm with excellent precision ($> 90\%$) for primary classes and less accurate results, arguably due to the unbalance of the training set, for secondary classes where traces of other elements are expected (DAZ, DBZ, ...).

Indeed, a key characteristic of supervised machine learning techniques is their complete reliance on the training dataset. Thus, the performance is severely affected if the training dataset is unbalanced with underrepresented classes. Furthermore, several works use training datasets built from SDSS spectra with a higher resolution ($R \approx 1800$) than that of Gaia, and as a consequence, those artificial intelligence models can misinterpret some non atmospheric features in the XP spectra such as the observational noise. These two

reasons strongly justify exploring alternative unsupervised learning approaches. Recently, Kao et al. (2024), used an unsupervised dimensionality reduction technique called Uniform Manifold Approximation and Projection (UMAP) to classify the Gaia XP spectra of WDs with a previous $P_{WD} > 0.9$ filter in the GF+21 catalogue. The UMAP allowed them to project each vector of 110 XP coefficients in a 2D map or manifold where similar elements appears next to each other. Subsequently, they found a well defined island of similar WD candidates showing Ca and other metals in their Gaia XP spectra. As a result, their methodology allowed them to discover new 375 polluted white dwarfs candidates. We will discuss these works in more detail later and compare their results with our own.

In this work, we use a neural network-based dimensionality reduction algorithm called Self-Organizing Maps (SOM) (Kohonen 1982) where, given a nonlinear high-dimensional dataset, the input data is projected on a 2D grid map where similar elements fall into the same neuron. Here, the similarity is defined by a metric (e.g. Euclidean distance) so the unsupervised learning process aims to maximize the similarity between objects belonging to the same neuron at the same time it minimizes the similarity between objects within different neurons. Therefore, topology is naturally preserved: similar neurons are also grouped next to each other. Once the clustering process ends, each neuron is labeled by means of a template-matching procedure where a tag is assigned to the mean element of that neuron (the prototype) (Delchambre et al. 2023; Pallas-Quintela et al. 2023).

Consequently, SOMs combine the two major utilities of unsupervised learning: dimensionality reduction and clustering, unlike other algorithms that either perform only clustering (e.g. K-means) or only dimensionality reduction (e.g. t-SNE, UMAP). This double characteristic demonstrated SOMs to be a great artificial intelligence tool for object classification in different fields of Astronomy and Astrophysics (Torres et al. 1998; Naim et al. 2009; Geach 2012; Way and Klose 2012; Carrasco and Brunner 2014; Álvarez et al. 2022), as well as for outlier detection and analysis (Ordoñez-Blanco et al. 2010; Fustes et al. 2013a,b; Dafonte et al. 2018).

The manuscript is organised as follows: in §2 we present the methodology to filter out and classify the Gaia DR3 WD candidates with SOM. The key results of our unsupervised classification procedure are shown in §3 and the main conclusions of this work are summarized in §4.

2. METHODOLOGY

Most of the Gaia DR3 sources can be placed on an absolute G magnitude to $G_{BP} - G_{RP}$ color diagram. In [Gentile-Fusillo et al. \(2019\)](#) and [Gentile-Fusillo et al. \(2021\)](#) this CMD is used to identify WDs in Gaia Early DR3 by applying color and absolute magnitude cuts that correspond to the WD region in the Hertzsprung–Russell diagram.

Since belonging to that region is a necessary but not a sufficient condition to be a WD (e.g. QSOs are also blue and faint), [Gentile-Fusillo et al. \(2021\)](#) determined a probability of being a WD (P_{WD}) as a function of the position in the color-magnitude parameter space, by using a well-known sample of 22,998 spectroscopically confirmed WDs and 7124 contaminants identified by visual inspection in the SDSS and subsequently converted to normalized 2D Gaussians in order to obtain two continuous density maps (one for confirmed WDs and other for contaminants). Then the P_{WD} for a given candidate was computed by integrating its CMD Gaussian distribution with the map resulting of taking the ratio of the confirmed WD density map to the sum of both maps.

As a result of applying this methodology to Gaia EDR3, [Gentile-Fusillo et al. \(2021\)](#) computed a catalog of around 1.3 million candidates, of which $\approx 359,000$ are classified as high-confidence WDs by imposing a $P_{WD} > 0.75$ probabilistic cut. The GF+21 sample of WD candidates not only increased the number of WDs by an order of magnitude, but it also allowed to classify such a big sample in different spectral types by means of their Gaia XP spectra.

Gaia XP spectra are provided for ~ 220 million sources from mean low resolution ($R \approx 70$) spectrophotometry up-to-date, and therefore represents a valuable tool to study the astrophysical properties of a large amount of objects. Instead of fluxes per wavelength unit, Gaia provides 110 coefficients (55 for the BP and 55 for the RP spectra) corresponding to sets of basis functions resulting from multiplying Gaussian functions to Hermite polynomials ([Carrasco et al. 2021](#)). These coefficients uniquely define the spectra of each source, and therefore they can be used to study its spectral features ([Weiler et al. 2023](#)).

2.1. Initial sample

As a baseline, we use GF+21 sample, that is constructed by imposing the following color-magnitude cut to isolate the WD locus in the CMD:

$$G_{abs} > 6 + 5 \cdot (G_{BP} - G_{RP}) \quad (1)$$

Subsequently, a large list of quality filters over several astrometric and photometric parameters was applied until arriving at a sample of 1,280,266 sources within the

WD region with high-quality measurements (see §2.1. in [Gentile-Fusillo et al. \(2021\)](#) for more information about all of those quality filters).

Finally, since we completely rely on the morphology to classify the spectra, we have applied several additional filters to ensure the quality of the input data: i) (`phot_bp_n_obs` > 10) & (`phot_rp_n_obs` > 15), refer to the minimum number of CCD transits for BP and RP spectra, respectively, based on the recommendations in [Andrae et al. \(2023\)](#) to ensure a sufficient signal-to-noise ratio (S/N) for posterior spectral analysis. We consider that the asymmetry in the cuts for BP and RP minimum number of observations are suitable for WDs since the weakest metallic lines we aim to find, such as K I or Li I, are in the RP wavelength range, and therefore a better signal-to-noise ratio is required to identify them in comparison with the BP lines (Ca II, Na I) that have more S/N.; ii) `visibility_periods_used` > 10, being each visibility period a group of observations separated from the next one by at least 4 days, keeping in this way only those sources that have been astrometrically “well-observed” ([Lindegren et al. 2018](#)); iii) `|phot_bp_rp_excess_factor_corrected|` < 5 x `sigma_excess_factor` which, as explained in [Riello et al. \(2021\)](#), makes sure that the photometry of G_{BP} , G_{RP} , and G is consistent, avoiding any possible contamination from external sources in the same field-of-view.

Then, we retrieved the Gaia XP spectra of this sample by using the DataLink Gaia tool (<https://www.cosmos.esa.int/web/gaia-users/archive/datalink-products>) through the `astroquery` Python package ([Ginsburg et al. 2019](#)), downloading XP coefficients for 104,844 sources.

2.2. Kohonen’s Self-Organizing Maps

In contrast to other works where the GF+21 catalog is used, here we did not appeal to the P_{WD} parameter to filter out contaminants. While we agree that this probabilistic cut discards the majority of contaminants from the initial sample, it relies only on the G , G_{BP} , and G_{RP} magnitudes. Since the XP coefficients encode much more information about the astrophysical properties of the Gaia sources, such as absorption and emission lines (key features to identify contaminants such as QSOs, [De Angeli et al. 2023](#)), they are more valuable to obtain a more conservative sample of bona fide WDs. To tackle this issue, we applied our own SOM approach to cluster WDs and contaminants in different neurons.

The learning process of SOM, as explained in the original implementation of [Kohonen \(1982\)](#), starts with a random initialization of the weights $w_{m,n}$ for each neuron $z_{m,n}$, being $m \times n$ the predefined dimension of the

map. Then, for each input element x_i , an initial iteration looks for the winner neuron (best matching unit, or BMU) by minimizing the Euclidean distance between x_i and each $w_{m,n}$. Subsequently, an iterative process updates the weights by means of a neighborhood function that preserves the topology with closer neurons. The learning process stops when the weights do not change significantly between iterations.

In pursuit of applying the SOM algorithm to the selected spectra, we chose the `MiniSom`¹ library in Python due to its simplicity and hyperparameter flexibility (Vetigli 2018). After some hyperparameter tuning, we selected the Euclidean as the activation distance, the Gaussian as the neighborhood function, and an initial learning rate of 0.7. Another important parameter is σ , which gives the initial spread of the neighborhood function so that a greater σ will consider farther neurons as neighbours while a smaller σ will only look at the closer ones. Finally, it should be noticed that such as any algorithm that depends on a distance calculation, it is very sensitive to the scale of the features (here, the XP coefficients), so to ensure a good performance we normalize each input vector of XP coefficients by dividing it by its \mathcal{L}_2 norm before the learning process.

2.3. Filtering out of contaminants

In order to clean our initial sample from non-WD objects that could share the locus defined in Equation (1) with true WDs, we use the same Gaia-SDSS spectroscopic sample published in GF+21 and available online². This sample contains 42,007 SDSS DR16 spectra of 32,321 sources. Here we only use those that pass the quality filters mentioned in §2.1 and with available XP spectra. As a result, we obtained a final sample of 10,835 sources, divided in 10,141 confirmed WDs and 694 contaminants labeled with any of the following tags: CV, DB_MS, DA_MS, DA_MS:, DC_MS, STAR, QSO, Unreli, UNKN, GALAXY, DA_DQ. In Figure 1 the Gaia-SDSS spectroscopically confirmed WDs (blue) and contaminants (red) are shown in a CMD.

To obtain reliable statistics we need to use synthetic data, since the sample size of contaminants is much smaller than that of confirmed WDs, with a poor ratio of 0.06. For this purpose, we use the Synthetic Minority Oversampling Technique (SMOTE) through the `imbalanced-learn`³ Python library (Lemaître et al. 2017) over the normalized XP coefficients, with a resam-

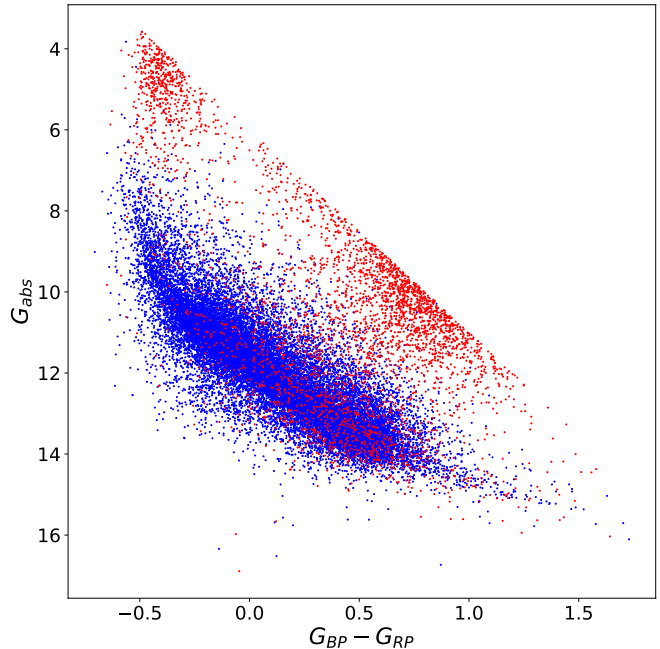


Figure 1. CMD of Gaia-SDSS spectroscopically confirmed white dwarfs (blue) and contaminants (red).

pling ratio of 0.20 for the minority class (10,141 confirmed WDs versus 2028 contaminants). The random seed for SMOTE as well as for the random initialization of the following SOMs was set to 1. With this resampled dataset we proceeded to train a SOM by choosing a small map size of 5×5 in order to have enough stars within each neuron. The number of iterations was 5×10^4 , with $\sigma = 1.5$, and a learning rate of 0.5.

The Self-Organized Map obtained is shown in Figure 2, where contaminants are depicted in red colors. As can be seen in the figure, there are neurons with different levels of contamination. While in the neuron $z_{0,4}$ the confirmed WDs are indistinguishable from the contaminants, $z_{3,3}$ just has a few of them. Thus, if we define the purity of a neuron as the ratio of the number of spectroscopically confirmed WDs to the total number of sources within that neuron, out of 25 neurons, 18 have a purity level greater than 90%.

A total of 7338 sources ($\sim 60\%$) fell into those neurons, of which the expected $< 10\%$ of contaminants correspond to 150 SDSS labeled sources completed with 269 unlabeled synthetic contaminants. From the labeled SDSS sources, only 18 are confirmed stars (STAR), 79 correspond to SDSS sources with unreliable spectral class, 1 is tagged as UNKN and the rest of them are CV (19 sources) and WD-main sequence binaries (33 sources). Therefore, no contaminants such as QSOs or galaxies are expected by using our method.

¹ <https://github.com/JustGlowing/minisom/>

² https://warwick.ac.uk/fac/sci/physics/research/astro/research/catalogues/gaiaedr3_wd_sdssspec.fits.gz

³ <https://imbalanced-learn.org>

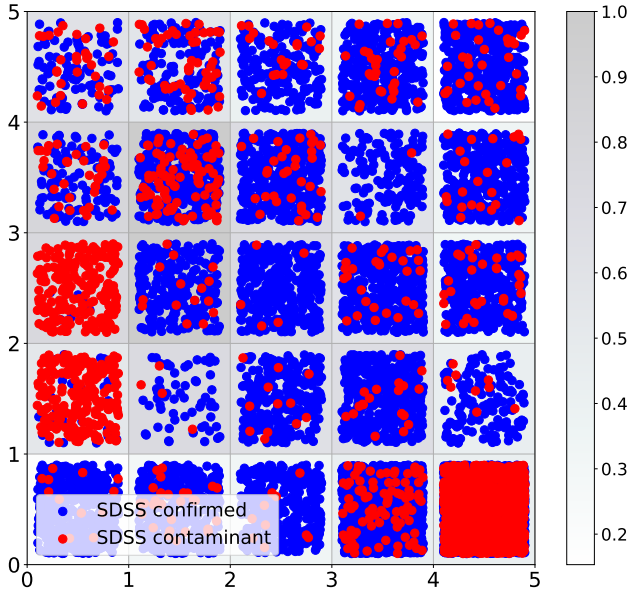


Figure 2. Self-Organized map of the Gaia-SDSS spectroscopic sample after 5×10^4 iterations. SDSS confirmed WDs are shown in blue and SDSS and synthetic contaminants in red. The side bar shows the Intra-Neuron Distance (IND) or how similar are the objects within the same neuron.

Once the map has been pre-trained (meaning that the final weight of each neuron has been computed with the XP coefficients of the Gaia-SDSS sample) we pass the initial sample defined in subsection 2.1 through the map, so that each vector of XP coefficients falls within the neuron to which the weight is closest. As a result, 66,337 sources ($\sim 63\%$) fell into our pure neurons.

2.4. Spectral classification

In order to classify the Gaia WD spectra, we have passed the 66,337 clean sources selected as WDs through a 8×8 SOM with the same hyperparameters as in §2.3 except that we use $\sigma = 1$ here, so that the algorithm discriminates more and thus increases precision. With the aim to give labels to each neuron, we cross-matched this sample with the Montreal White Dwarf Database (MWDD)⁴ (Dufour et al. 2016) and separate them in the six primary spectral classes: DA, DB, DO, DQ, DZ and DC, referring to the main chemical abundances present in their atmospheres. The resulting map is shown in Figure 3, where only the 9273 WDs with confirmed classification in the MWDD are colored, being 7088 DAs, 933 DCs, 634 DBs, 340 DZs, and 278 DQs. There are not DOs after the SOM filter, so from now on we will not deal with them. The remaining 57,064 DNC (short for

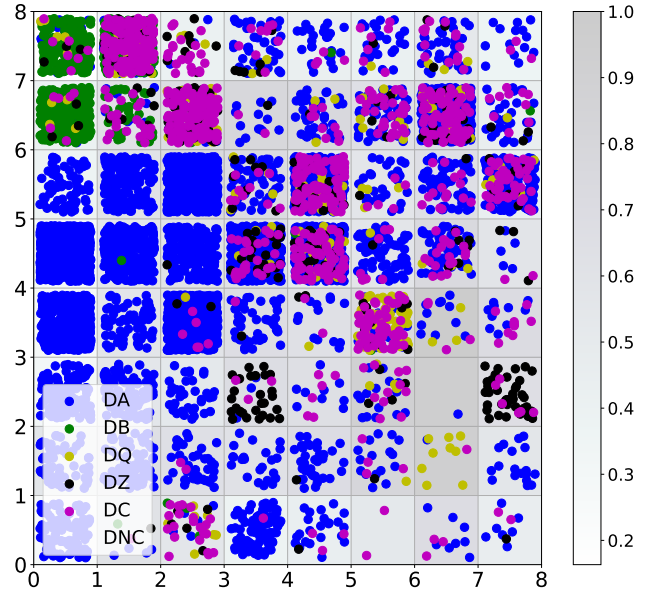


Figure 3. SOM map with our sample of 66,337 clean sources. WDs with known spectral type in MWDD catalog appear in different colors, and candidates are invisible to enhance visualization.

‘Not Classified’) candidates are invisible for the sake of visualization.

Subsequently, we used the most frequent class within each neuron as its representative class, if and only if the ratio of that class with respect to the others is of 0.5 or higher. We have chosen 0.5 because we aim to use the most frequent class as the representative label of that neuron but, at the same time, there are neurons where the ratio of the classes is too spread out to state with certainty that all the stars in that neuron belong to the most frequent class. Therefore, setting a minimum threshold is highly recommended. Otherwise, the neuron is classified as Outlier since it contains too mixed classes and no high-precision classification would be reliable. By applying this filter, 60 neurons are considered useful for classification, accounting for 61,817 WDs, and only four of them ($z_{1,6}$, $z_{1,7}$, $z_{5,2}$, and $z_{5,3}$) are labeled as Outlier.

3. RESULTS AND DISCUSSION

3.1. WD candidates

Regarding the filter of contaminants applied in this work, from the 66,337 clean sources, 1804 have a $P_{WD} < 0.9$ while 791 sources have $P_{WD} < 0.75$ in Gentile-Fusillo et al. (2021), showing that the use of Gaia XP coefficients instead of Gaia CMD has allowed us to reveal new candidates. Furthermore, 84% of the contaminants are sources that are considered in the GF+21 catalog as high-confidence WD candidates (they have

⁴ <https://www.montrealwhitedwarfdatabase.org/>

$P_{WD} > 0.75$). We certainly have imposed a quite conservative filter in order to get the purest sample. Therefore, in exchange for precision, it is expected that we are considering quite a few true WDs as contaminants. However, we also find that a very important fraction of the high confidence WD candidates in GF+21 have XP spectra morphologically similar to contaminants such as stars and QSOs. Thus, care must be taken.

One of the main limitations of the SOM is its recall, since the objective of this work is to obtain a the most pure sample, and therefore conservative filters are prioritized. As a consequence, in the sample of 38,507 sources classified as contaminants in §2.3, there are 14,376 (37%) sources in the MWDD and 5844 (15%) of them have a confirmed spectral type. Taking into account the total number of WDs from each MWDD spectral type in our initial sample, we can roughly estimate that we are missing 38% of DAs, 47% of DBs, 42% of DCs, 19% of DZs, 25% of DQs, and 100% of DOs by applying our SOM filter. Fortunately, the DZs that are the spectral type we are most interested in hunting are also the less affected ones.

We applied the Equation 2 of Golovin et al. (2024) to the sample of sources within 50pc to the Sun (see Equation 1 in the same paper) selected by the SOM filter as WDs (743 sources), in order to see if they may be contaminants due to spurious astrometric solutions. All those sources passed correctly the filter. The same was applied for the sources classified as contaminants by the SOM within the same distance (1405 sources), finding that three of them are also considered contaminants in Golovin et al. (2024).

We have also studied the distribution of parallax relative errors in both the 66,337 WD candidates and in the sample of 38,507 sources classified as possible contaminants. We found that while only 291 of the WD candidates ($\sim 0.7\%$) have a parallax relative error (σ_ω/ω) $> 10\%$, this number increases significantly to 2949 for the contaminants ($\sim 8\%$ of them). Thus, part of the contamination is most likely due to the fact that poor parallaxes introduce errors in G_{abs} , and as a consequence in the position of the source in the HR diagram. Notwithstanding that, and as can be seen in Figure 4, most of the sources classified as contaminants show good parallaxes as well.

This could suggest that most of the sources classified as contaminants are actually true WDs. However, several types of contaminants, such as unresolved binaries, can still appear in the WD locus despite being correctly identified as contaminants. As a result, the parallax error cut may not be sufficient to effectively eliminate contamination in large samples of WD candidates. The

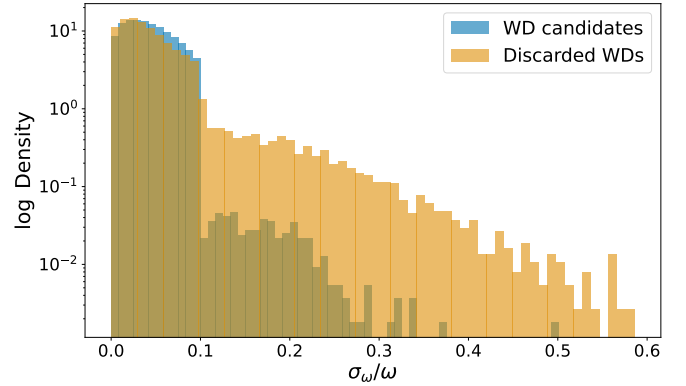


Figure 4. Parallax relative error distribution (density in log scale) of the 66,337 WD candidates and of the 38,507 sources classified as possible contaminants.

Table 1. Precision and recall metrics for each primary spectral class.

Class	Precision	Recall
DA	0.90	0.97
DB	0.84	0.65
DC	0.53	0.19
DQ	0.82	0.03
DZ	0.85	0.20

data analyzed in this study is still insufficient to draw definitive conclusions.

3.2. Spectral classification

Once we have assigned a label to each neuron (and therefore to each WD falling in that neuron), we can compare the predicted class with the true class given by the MWDD by using a confusion matrix C such the one shown in Figure 5. The number in each cell $C_{i,j}$ shows the number of WDs with a true label i and a predicted class j . Immediately below is shown the same quantity, but normalized over the predicted labels (columns) so the precision of the classification for each class appears in the diagonal. Thus, the confusion matrix would be diagonal for an ideal classification. Our confusion matrix shows excellent precision for DA and DZ classes ($\geq 85\%$), very good precision for DB and DQ classes ($\geq 80\%$), and poor metrics for DC class that is mainly confused with DAs and Outliers. In addition, Outlier neurons are mainly populated with a mixture of all classes but mainly with DCs and DBs. Recall is excellent for DAs but poor for the rest of the classes. In Table 1 the precision and recall metrics obtained for each class are summarized.

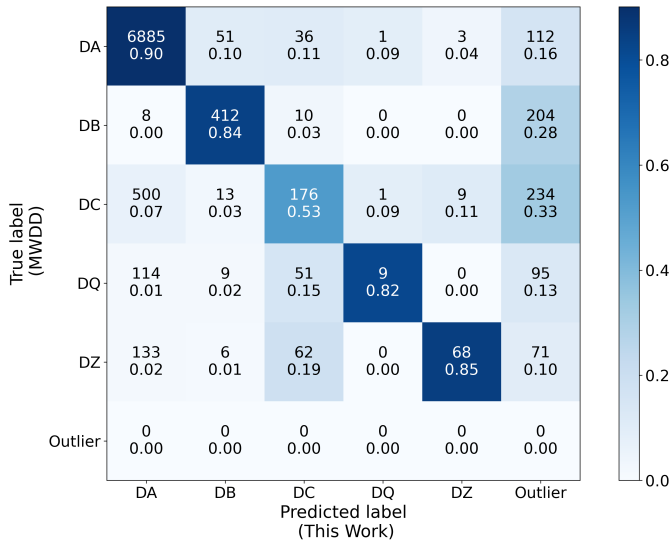


Figure 5. Confusion matrix of the SOM classification for WD primary spectral types with respect to MWDD classification.

Figure 6 shows the distribution of the G -band magnitude for those 9273 WDs with a confirmed spectral class in the MWDD and for our 57,064 DNC candidates. As can be seen, the apparent magnitude is more concentrated in the second case, something expected since the MWDD WDs were observed using different facilities with a wider range of telescope sizes and limiting magnitudes. In any case, the G -band magnitude is not very different in DNC candidates (mainly contained within [16, 20] mag) from the MWDD confirmed ones, so the DNC candidate classified spectra is not expected to be noisier. This is a necessary condition for good SOM performance. Otherwise, the morphological features produced by the noise can be interpreted as real spectral features by the SOM and these spectra could be incorrectly classified.

To visualize the reliability of the classification, we have plotted the median externally calibrated spectrum of several spectral classes using the `GaiaXPy`⁵ Python library (Ruz-Mieres 2024). In Figure 7a, a comparison between the normalized median spectra of 972 MWDD confirmed DAs and that of 4379 DA candidates in neuron $z_{0,4}$ are shown overlapped. The H Balmer lines ($\lambda 397.0$, $\lambda 410.2$, $\lambda 434.0$, $\lambda 486.1$, $\lambda 656.3$; units in nanometers) are plotted as dashed vertical lines. The same is done for the 253 confirmed DBs and 1478 DB candidates in neuron $z_{0,6}$ (Figure 7b) with their ex-

⁵ <https://www.cosmos.esa.int/web/gaia/gaiaxpy>

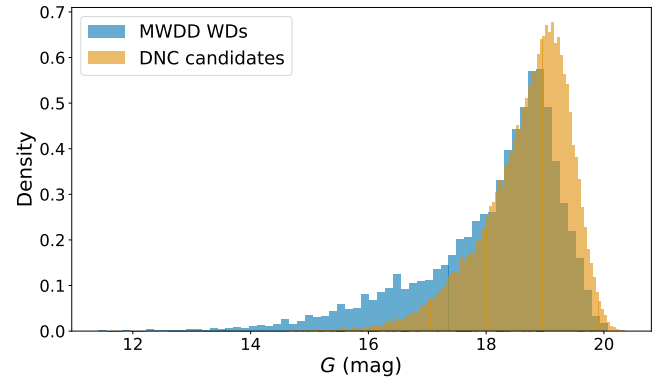


Figure 6. Density histograms of G -band magnitude for WDs with confirmed spectral classification and WD candidates. No differences between spectral classes were observed.

pected He I lines ($\lambda 388.9$, $\lambda 447.1$, $\lambda 587.6$). For DQ class, we used the neuron $z_{6,1}$ that, since it only contains 9 confirmed DQ sources with respect to 81 DQ candidates, looks noisier, as can be seen in Figure 7c where some Carbon lines for guidance are included. For DC class, we plotted the median spectra of the neuron $z_{2,6}$ that, as can be seen in Figure 7d, is mainly featureless.

Regarding the polluted WDs, they are mainly concentrated in neurons $z_{3,2}$ (hereafter, DZA neuron, with 249 sources) and $z_{7,2}$ (hereafter, DZ neuron, with 218 sources). In Figure 8a the normalized median spectra of 68 MWDD confirmed DZs is shown overlapped to the normalized median spectra of the 399 DZ candidates. Furthermore, the desired Ca II H+K doublet ($\lambda 393.4$, $\lambda 397.9$) is clearly seen in both.

However, while both neurons are mainly populated by WDs labeled in the MWDD as DZs ($\sim 80\%$ and $\sim 90\%$, calculated with respect to the total number of WDs with MWDD classification, respectively) the first one is mixed with $\sim 20\%$ of MWDD DAs and DCs in equal parts, and the second one with $\sim 10\%$ of DCs. These indicate that other features than Calcium may be present in these Gaia XP spectra. In Figure 8b the normalized median spectra of both neurons is plotted independently (DZA neuron in blue, and DZ neuron in orange) with several absorption lines for guidance. Lines in common are plotted in black, those only found in the DZA neuron in blue, and those specific to the DZ neuron in orange.

Besides the Ca II H&K doublet, the median spectra (Figure 8b, in blue), shows a plenty of H Balmer lines ($\lambda 434.0$, $\lambda 486.1$, and $\lambda 656.3$) indicating a population of H-rich polluted WDs in that neuron (hereafter, DZA neuron). An extra Ca II ($\lambda 373.7$) dash-dotted line and two more metals are present in the spectra, according to the features in the $\lambda 517.3 - 518.3$ Mg I triplet and

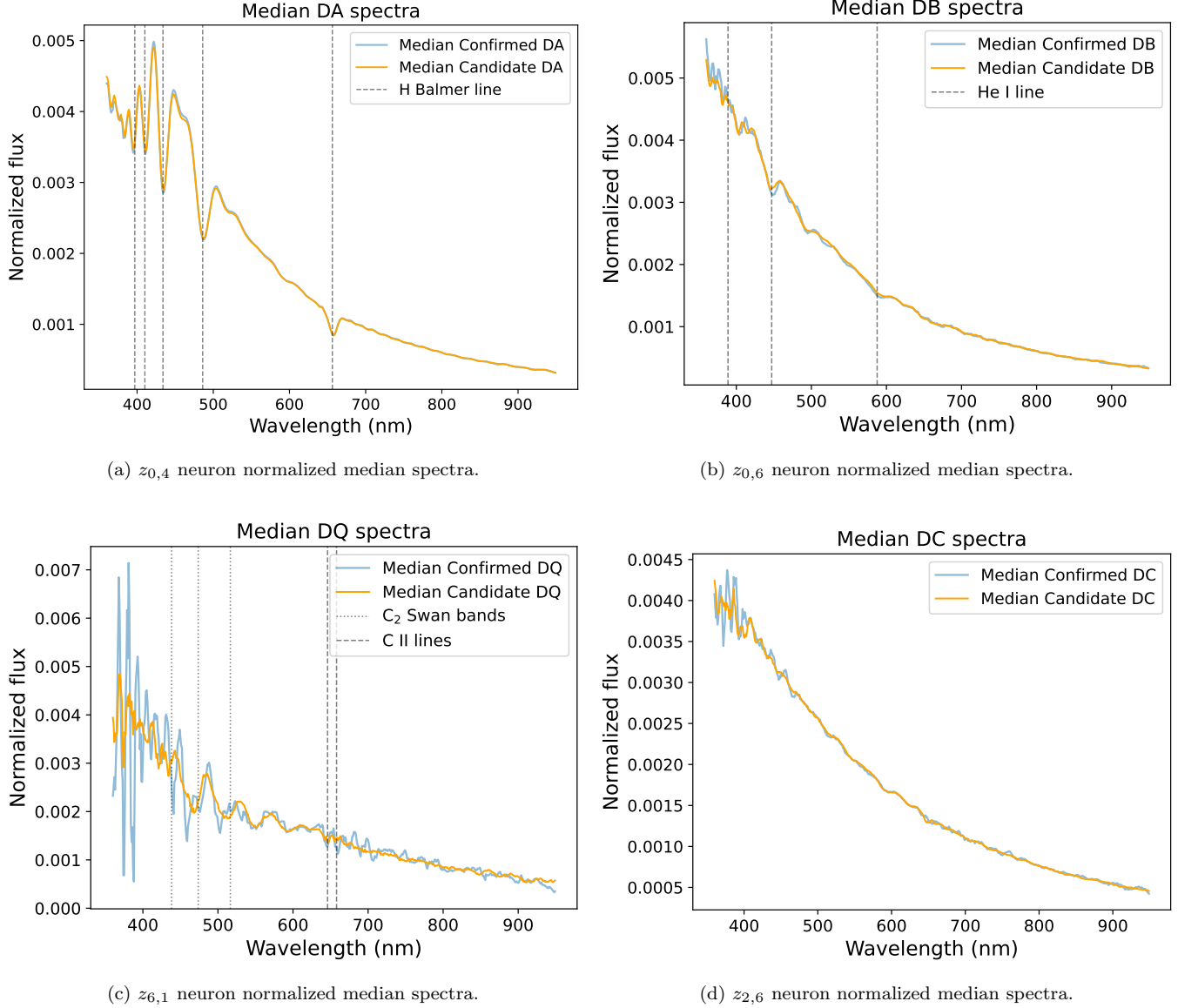


Figure 7. Normalized median spectra of WDs with confirmed spectral classification in the MWDD and identified candidates for several neurons.

in the $\lambda 589.0 - 589.6$ Na I doublet. Regarding the $z_{7,2}$ median spectra, we can see in Figure 8b (in orange) how the Balmer series disappeared, at the same time that other metals came to light, as suggested by the presence of the Ca I line ($\lambda 423.0$) and possible detections of Li I and K I doublets around $\lambda 670.8$ and $\lambda 766.5 - 769.9$, respectively. The absence of H and He I lines indicates that this neuron (hereafter, DZ neuron) may be populated by cool DZs.

Indeed, the T_{eff} distribution (obtained from Gentile-Fusillo et al. (2021), by assuming mixed H and He atmospheres), is greater in the DZA neuron, ranging from 7200 K to 28,600 K, with a mean of 9200 K. On the other side, the T_{eff} distribution in the DZ neuron ranges

from 6600 to 12,000 K, with a mean of 7200 K, which explains the absence of He I lines since below 11,000 K there is not enough temperature to excite them, making the $z_{7,2}$ a cool DZ neuron. Metals displayed in the atmospheres of cool polluted WDs had to be accreted, as well as in almost all of WDs in the DZA neuron, since with a temperature $< 25,000$ K the radiative levitation could not be the cause (Chayer et al. 1995). In Figure 9 we show the T_{eff} density distribution for each neuron, with the DZA neuron values up to the 99th percentile (corresponding to $T_{eff} < 14,400$ K) to enhance visualization.

3.3. Comparison with other methodologies

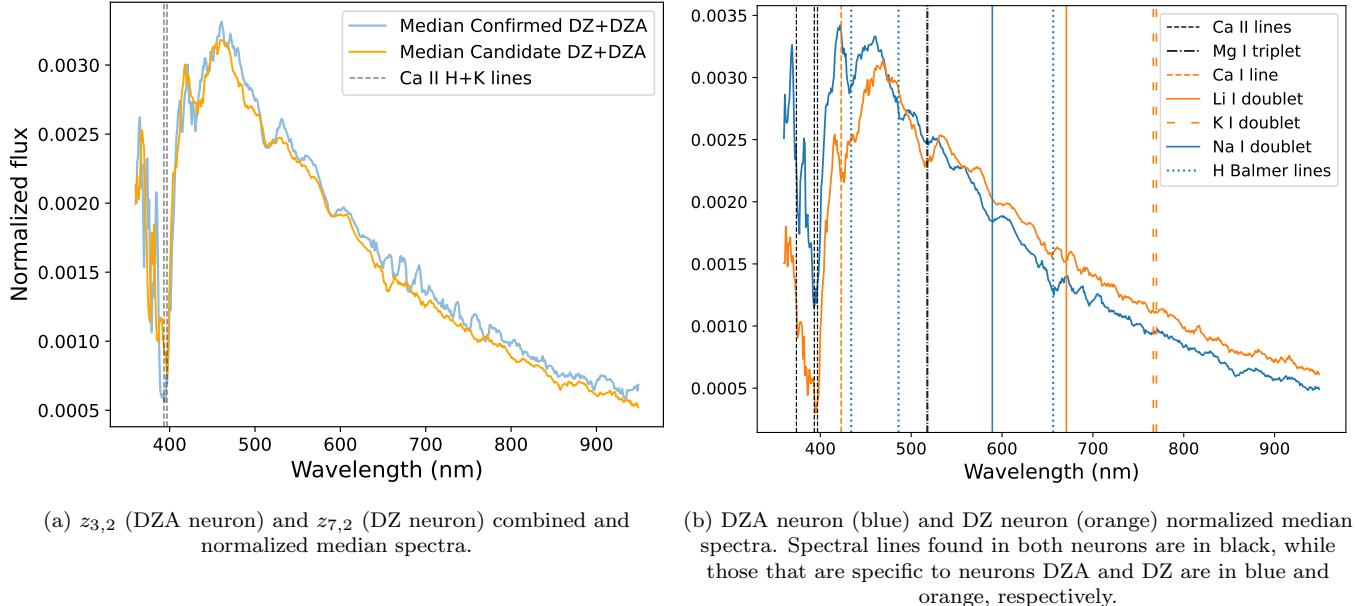


Figure 8. Normalized median spectra for the neurons with identified polluted WDs.

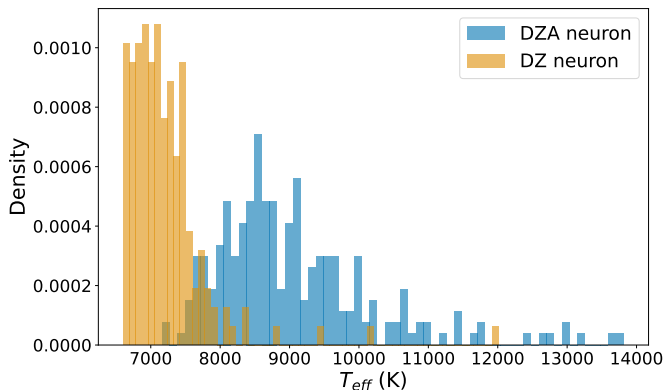


Figure 9. Density histograms of T_{eff} assuming mixed H and He atmospheres from [Gentile-Fusillo et al. \(2021\)](#) for DZA and DZ neurons in bins of 100 K.

We have also compared our classification with supervised learning methods such as that of the [García-Zamora et al. \(2023\)](#) and [Vincent et al. \(2024\)](#). [García-Zamora et al. \(2023\)](#) trained a Random Forest algorithm with MWDD labels to classify the WD 100 pc volume-limited sample of [Jiménez-Esteban et al. \(2023\)](#), while [Vincent et al. \(2024\)](#) used an ensemble algorithm of decision trees, to classify the [Vincent et al. \(2023\)](#) sample.

To compare the results of our method with these supervised classifications, we cross-matched their catalogs with ours. 4662 WDs were found to be in common between [García-Zamora et al. \(2023\)](#) and our SOM. Since some of the candidates have secondary class classification in their catalog, we considered only their primary classification (so DAB, DAH, DAZ, ... are all consid-

ered as DAs; DBAs, DBZs, ... are all considered as DBs; and so on). On the other hand, [Vincent et al. \(2024\)](#) shows 56,617 candidates classified with reliable primary spectral types i.e., not classified by the authors as uncertain (indicated by a ":" notation) that are also in our catalog. The confusion matrices, with our labels considered as the predicted labels, are shown in Figures 10a and 10b, respectively.

As can be seen, our results reveal a very good precision with respect to those of [García-Zamora et al. \(2023\)](#) except for our DBs, since a 30% of them are classified in their work as DCs. On the other hand, the confusion matrix of our work with [Vincent et al. \(2024\)](#) is nearly diagonal, showing also a good precision for all of the classes. Notwithstanding that, an excellent agreement requires an excellent recall, that is the main limitation of our SOM as stated before, and shown again here.

Indeed, we can see that, for instance, we identified a total of 72 DZs in the cross-match with [García-Zamora et al. \(2023\)](#), of which 58 are classified by them as DZs (81%), 11 as DCs and 3 as DAs. However, of the 167 DZs in [García-Zamora et al. \(2023\)](#), we only classify as such 58 of them (35%), since more than a half are classified by the SOM as DAs. The same scenario occurs with [Vincent et al. \(2024\)](#) cross-match, where of the 423 WD candidates identified as DZs by the SOM, 302 (71%) are also classified as DZs in their work. However, of the 840 WDs labeled as DZs by them, only 302 are identified as DZs in our work (36%).

This results are in high consonance with those shown in §3.2 (see Figure 5 and Table 1) and reinforce the fact

that the main strength of the SOM is its high precision, but at the cost of having a very low recall.

Of the 467 sources classified as polluted, 136 were found in the Montreal White Dwarf Database but only 68 have been classified as polluted WDs up to the 3rd of July 2024. Of the remaining 399 DZ candidates, 37 (9%) were classified as DZ in [García-Zamora et al. \(2023\)](#), and 236 (59%) in [Vincent et al. \(2024\)](#) (36 of them are also in common with [García-Zamora et al. 2023](#)).

We have also cross-matched our sample with the polluted WD catalog of [Badenas-Agusti et al. \(2024\)](#) and two only sources matched with our sample, they are also in [García-Zamora et al. \(2023\)](#) and [Vincent et al. \(2024\)](#).

During the preparation of this manuscript, [Kao et al. \(2024\)](#) used UMAP to perform an unsupervised classification of the GF+21 catalog, obtaining a sample of 375 polluted candidates. Although they did not publish that sample in their paper, they provide the UMAP projected 2D coordinates for each source. Thus, we were able to cross-match their catalogue with our sample.

Of our 467 DZ candidates, 456 of them have positions in their UMAP, and nine of the remaining 11 are not in the previous catalogs. In [Figure 11](#) we show the UMAP of [Kao et al. \(2024\)](#) in blue and our DZ and DZA candidates in red and orange, respectively. As can be seen in [Figure 4](#) of their work, the polluted WDs they have found are concentrated in a DZ island in the UMAP. Our DZ and DZA candidates are distributed through that island but also in other parts of the UMAP so they are not in the [Kao et al. \(2024\)](#) DZ sample.

To roughly determine how many of our candidates are actually new WD candidates, we have set the following conditions (2) and (3) for the UMAP coordinates (UMAP1 and UMAP2) so that we filtered the candidates of our sample that are below the two black dotted lines depicted in [Figure 11](#) and that wrap around the DZ island:

$$\text{UMAP2} < 2.44 \times \text{UMAP1} - 8.02, \text{ if } \text{UMAP1} \geq 3.20 \quad (2)$$

$$\text{UMAP2} < -0.50 \times \text{UMAP1} + 1.40, \text{ if } \text{UMAP1} < 3.20 \quad (3)$$

We find that from the 456 of our polluted WD candidates that are in the UMAP, 225 sources (13 DZ candidates and 212 DZA candidates) are out of the [Kao et al. \(2024\)](#) DZ island. Moreover, the candidates in the DZ neuron have more metal species identified in their Gaia spectra than those of the DZA neuron, which explains that we have more of them in common with their work, since they also found up to five different metal species.

This together with all of the cross-matches that we have described before, gives us confidence to report that at least 143 of our polluted WD candidates (133 DZAs and 10 DZs) are completely new discoveries.

As mentioned before, (see [Table 1](#) as well), the main limitation of the SOMs presented in this work is their lack of sensitivity or recall, mainly because of the labeling procedure. Despite of that, we demonstrated here that both the SOM filter as well as the classification SOM were able to recover many high-confidence polluted WDs that previous supervised and unsupervised learning works overlooked. Indeed, the combination of dimensionality reduction and clustering skills of the SOM allowed to identify a population of new DZA candidates that the UMAP missed.

Another important advantage of the clustering characteristic in the SOM is that it allows us to perform statistics within each neuron in order to obtain a golden sample with only the best candidates for each spectral class.

For instance, if we compute the intra-neuron distance (IND) distribution for each neuron as the distance of each spectrum to the mean spectrum of that neuron, we can obtain an internal validation of our procedure: a neuron is a reliable cluster if and only if the INDs are low, showing an assymetric left-skewed Gaussian shape. [Appendix 1](#) displays, in [Figure 12](#), the distribution of distances achieved by mapping our sample of 104,844 sources to the SOM map pretrained with SDSS sources in [Figure 2](#), while in [Figure 13](#) we show the IND distribution for each neuron in the map presented in [Figure 3](#). The distance distribution mirrors that of the original maps, demonstrating the method’s effectiveness and enabling reliable classification. Moreover, we can choose the most reliable objects as those that have the lowest INDs within their own neuron.

This work outlines the methodology used to identify a set of bona fide polluted WD candidates, detailing the steps taken to ensure the work’s reproducibility. The list of candidate objects will be validated with high-resolution observations.

4. CONCLUSIONS

We have demonstrated in this work the power of unsupervised learning to filter data by obtaining a clean sample of 66,337 WD candidates from the Gaia white dwarf catalog of [Gentile-Fusillo et al. \(2021\)](#) using alternative input data (Gaia XP spectra instead of the Gaia CMD) and methodology (unsupervised machine learning with SOM). This has led us to a less complete but more robust and high-confidence sample of WDs, as the XP coefficients store more information than just G , G_{BP} , G_{RP} magnitudes. By applying the SOM algorithm to the GF+21 sample of WD candidates with Gaia XP spectra as input data, we can exclude contaminants in a more robust and reliable way than by using

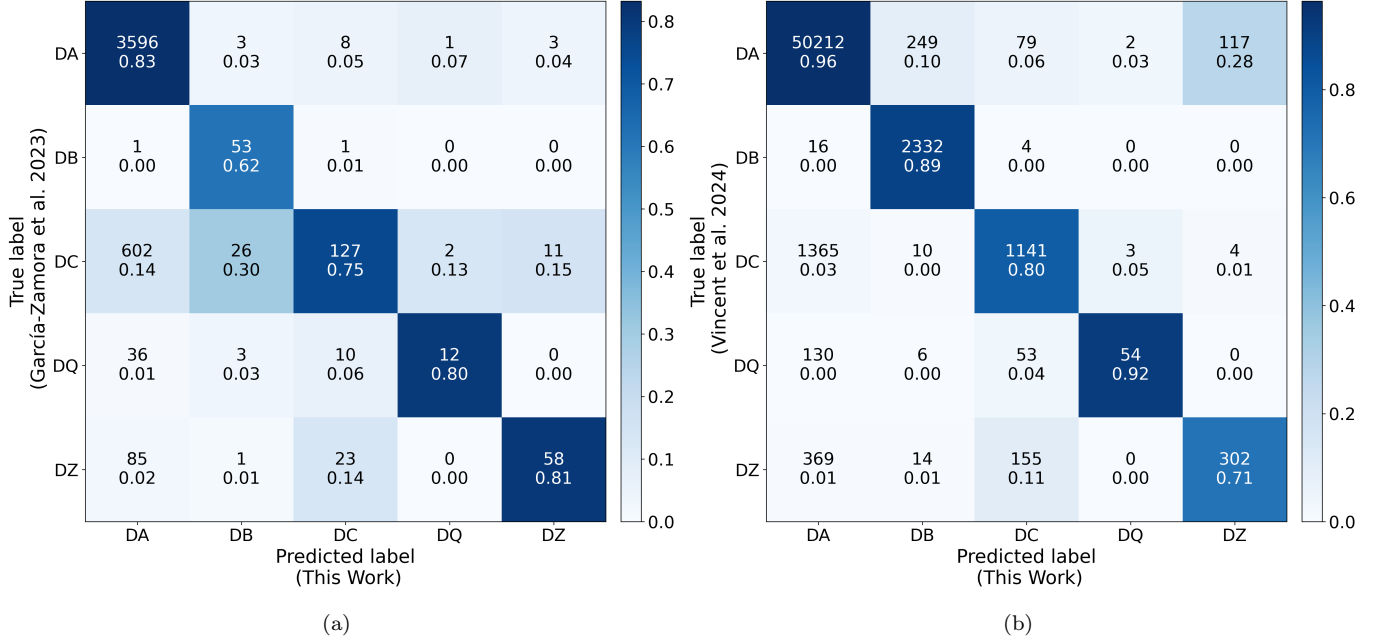


Figure 10. Confusion matrices of our work (the predicted labels) with [García-Zamora et al. \(2023\)](#) (a) and [Vincent et al. \(2024\)](#) (b) (the true labels). The numbers in each cell have the same meaning as those in Figure 5.

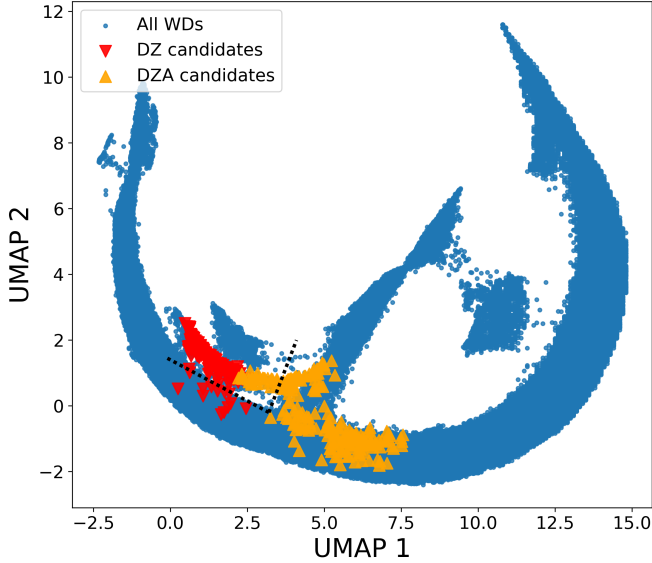


Figure 11. UMAP of [Kao et al. \(2024\)](#) with all of their WD candidates in blue and our DZ and DZA candidates in red and orange, respectively. The black dotted lines served us to discriminate the polluted WD candidates identified in their work from those identified here.

the P_{WD} , which is solely based on the position of the candidate in the H-R diagram, as well as classify the true WDs according to their spectral morphology. Moreover, the fact that 791 sources of our sample appear as low-

confidence ($P_{WD} < 0.75$) WDs in the GF+21 catalog proves our methodology to be a useful tool for identifying hidden but reliable WDs.

Regarding the spectral classification, unsupervised Self-Organizing Maps have shown a similar performance that in recent supervised learning works, with high precision for DA, DB, DQ, and DZ white dwarfs. This strongly justifies the use of Self-Organizing Maps as they provide a natural and useful way to group similar spectra and, at the same time, to label new data, by performing statistics within each neuron.

This method allowed us to identify, with high confidence, 143 new polluted WD candidates that show spectral features of several metals (namely, Ca, Mg, Na, Li, and K), and even to distinguish between DZ and DZA subtypes. In order to confirm those candidates and to delve into other interesting neurons (such as DQ and DXZ subtypes) follow-up spectroscopy of the best candidates will be performed in the near future.

We warmly thank the anonymous referee whose insightful comments have greatly improved this paper. This work has made use of data from the European Space Agency (ESA) Gaia mission and processed by the Gaia Data Processing and Analysis Consortium (DPAC). Funding for the DPAC has been provided by national institutions, in particular the institutions participating in the Gaia Multilateral Agreement. This work has made use of the Python package GaiaXPy, developed and maintained by members of the Gaia Data Processing and Analysis Consortium (DPAC) and in particular, Coordination Unit 5 (CU5), and the Data Processing Centre located at the Institute of Astronomy, Cambridge, UK (DPCI). This research was funded by the Horizon Europe [HORIZON-CL4-2023-SPACE-01-71] SPACIOUS project, Grant Agreement no. 101135205, the Spanish Ministry of Science MCIN / AEI / 10.13039 / 501100011033, and the European Union FEDER through the coordinated grant PID2021-122842OB-C22. We also acknowledge support from the Xunta de Galicia and the European Union (FEDER Galicia 2021-2027 Program) Ref. ED431B 2024/21, ED431B 2024/02, and CITIC ED431G 2023/01. X.P. acknowledges financial support from the Spanish National Programme for the Promotion of Talent and its Employability grant PRE2022-104959 cofunded by the European Social Fund. Funding from Spanish Ministry project PID2021-127289NB-100 is also acknowledged.

REFERENCES

- Álvarez, M.A., Dafonte, C., Manteiga, M. et al. 2022, *Neural Comput & Applic*, 34, 1993–2006
- Andrae, R., Fouesneau, M., Sordo, R., et al. 2023, *A&A*, 674, id.A27, 22.
- Badenas-Agusti, M., Vanderburg, A., Blouin, S., et al. 2024, *MNRAS*, 527, 4515. doi:10.1093/mnras/stad3362
- Carvalho, A., Marinho Jr., R. M., Malheiro, M., et al 2016, *J. Phys.: Conf. Ser.* 706 052016
- Carrasco, K. M., Brunner, R. J. 2014, *MNRAS*, 438(4), 3409–3421
- Carrasco, J. M., Weiler, M., Jordi, C., et al. 2021, *A&A*, 652, A86
- Chayer, P., Fontaine, G., & Wesemael, F. 1995, *ApJS*, 99, 189. doi:10.1086/192184
- Dafonte, C., Garabato, D., Álvarez, M.A., Manteiga, M. 2018, *Sensors*, 18, 1419
- De Angeli, F., Weiler, M., Montegriffo, P., et al. 2023, *A&A*, 674, A2
- Delchambre, L., Bailer-Jones, C. A. L., Bellas-Velidis, I., et al. 2023, *A&A*, 674, A31. doi:10.1051/0004-6361/202243423
- Dufour, P., Blouin, S., et al. 2016, arXiv:1610.00986 [astro-ph.SR]
- Echeverry, D., Torres, S., Rebassa-Mansergas, A., et al. 2022, *A&A*, 667, A144
- Farihi, J., Barstow, M. A., Redfield, S., et al. 2010, *MNRAS*, 404, 2123
- Fustes, D., Dafonte, C., Arcay, B. et al. 2013, *Expert Syst Appl*, 40(5), 1530–1541.
- Fustes, D., Manteiga, M., Dafonte, C. et al. 2013, *A&A*, A7, 10.
- Vallenari, A., Brown, A.G.A., Prusti, T., et al. 2023, *A&A* 674, A1
- Garabato, D. 2020, PhD thesis. University of A Coruña
- García-Zamora E. M., Torres S., Rebassa-Mansergas A., 2023, *A&A*, 679, A127
- Geach, J. E. 2012, *MNRAS*, 419, 2633–2645
- Gentile Fusillo, N. P., Tremblay, P.-E., Gänsicke, B. T., et al. 2019, *MNRAS*, 482, 4570. doi:10.1093/mnras/sty3016
- Gentile Fusillo, N. P., Tremblay, P.-E., Cukanovaite, E., et al. 2021, *MNRAS*, 508, 3877. doi:10.1093/mnras/stab2672

- Ginsburg, A., Sipőcz, B. M., Brasseur, C. E., et al. 2019, *AJ*, 157, 98. doi:10.3847/1538-3881/aafc33
- Golovin, A., Reffert, S., Vani, A., et al. 2024, *A&A*, 683, A33. doi:10.1051/0004-6361/202347767
- Iben I. J., Ritossa C., Garcia-Berro E., 1997, *ApJ*, 489, 772
- Izquierdo, P., Toloza, O., Gänsicke, B. T., et al. 2020, *MNRAS*, 501(3), 4276-4288
- Jiménez-Esteban, F. M., Torres, S., Rebassa-Mansergas, A., et al. 2023, *MNRAS*, 518, 5106.
- Kao, M. L., Hawkins, K., Rogers, L. K., et al. 2024, *ApJ*, 970, 181. doi:10.3847/1538-4357/ad5d6e
- Klein, B. L., Doyle, A. E., Zuckerman, B., et al. 2021, *ApJ*, 914(1), id.61, 17
- Koester, D., Wilken, D. 2006, *A&A*, 453, 1051.
- Koester, D. 2009, *A&A*, 498(2), 517-525.
- Kohonen, T. 1982, *Biol. Cybern.* 43, 59-69
- Lemaître, G., Nogueira, F., Aridas, C. K. 2017, *JMLR*, 18(17), 1-5.
- Lindgren, L., Hernández, J., Bombrun, A., et al. 2018. *A&A*, 616, id.A2, 25
- Maldonado, R. F., Villaver, E., Mustill, A. J., et al. *MNRAS*, 499(2), 1854-1869
- Maldonado, R. F., Villaver, E., Mustill, A. J., et al. 2021. *MNRAS*, 501(1), L43-L48
- Mustill, A. J., Villaver, E., Veras, D., et al. 2018, *MNRAS*, 476(3), 3939-3955
- Naim, A., Ratnatunga, U., Griffiths, E. 2009, *ApJ Suppl Series* 111, 357
- Ordoñez-Blanco, D., Arcay, B., Dafonte, C. et al. 2010, *Lect Notes Essays Astrophys*, 4, 97-102
- Pallas-Quintela, L., Garabato, D., Manteiga, M., Dafonte, C. 2023, *Highlights of Spanish Astrophysics XI, Proceedings of the XV Scientific Meeting of the Spanish Astronomical Society held on September 4-9, 2022, in La Laguna, Spain.* M. Manteiga, L. Bellot, P. Benavidez, A. de Lorenzo-Cáceres, M. A. Fuente, M. J. Martínez, M. Vázquez Acosta, C. Dafonte (eds.)
- Pelletier, C., Fontaine, G., Wesemael, F., Michaud, G., Wegner, G. 1986, *ApJ*, 307, 242
- Riello et al. 2021, *A&A*, 649, id.A3, 33 pp.
- Ruz-Mieres, D. 2024, *gaia-dpci/GaiaXPpy: GaiaXPpy v2.1.2*, doi: 10.5281/zenodo.11617977
- Sion, E. M., Greenstein, J. L., Landstreet, J. D., et al. 1983, *ApJ*, 269, 253
- Swan, A., Farihi, J., Su, K. L-U., Desch, S. J. 2024, *MNRAS: letters*, 529(1), L41-L46
- Torres, S., García-Becerro, E., Isern, J. 1998, *ApJ*, 508, L71
- Trierweiler, . L., Doyle, A. E., Young, E. D. 2023, *PSJ*, 4(8), id.136, 13
- Veras, D., Mustill, A., Bonsor, A. 2024, *Reviews in Mineralogy and Geochemistry*, 90(1), 141-170
- Vettigli, G. 2018, <https://github.com/JustGlowing/minisom/>
- Vincent, O., Bergeron, P., Dufour, P. 2023, *MNRAS*, 521, 760
- Vincent, O., Barstow, M. A., Jordan, S., et al. 2024, *A&A*, 682, A5
- Way, M., Klose, C. 2012, *PASP*, 124
- Weiler, M., Carrasco, J. M., Fabricius, C., Jordi, C. 2023, *A&A* 671, A52
- Xu, S., Rogers, L., Blouin, S. 2024, *arXiv:2404.15425*
- Zuckerman, B., Koester, D., Melis, C., et al. 2007, *ApJ*, 671(1), 872-877

APPENDIX

A. INTRA-NEURON DISTANCE DISTRIBUTIONS

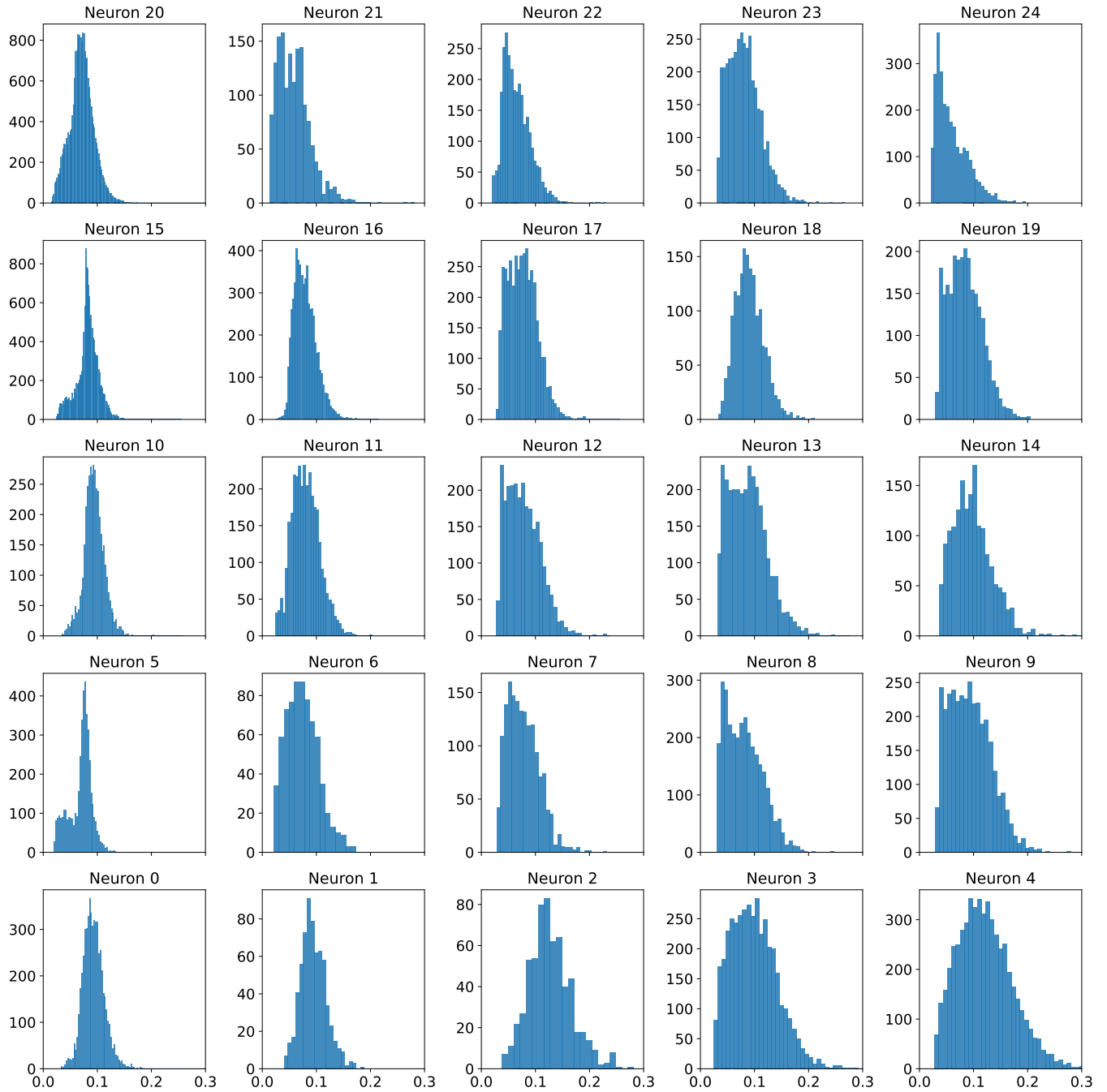


Figure 12. Intra-Neuron Distance distribution for the SOM used for filtering out contaminants from reliable WDs (see Figure 2). Neuron 0 is $z_{0,0}$, 1 is $z_{0,1}$, 5 is $z_{1,0}$, and so on.

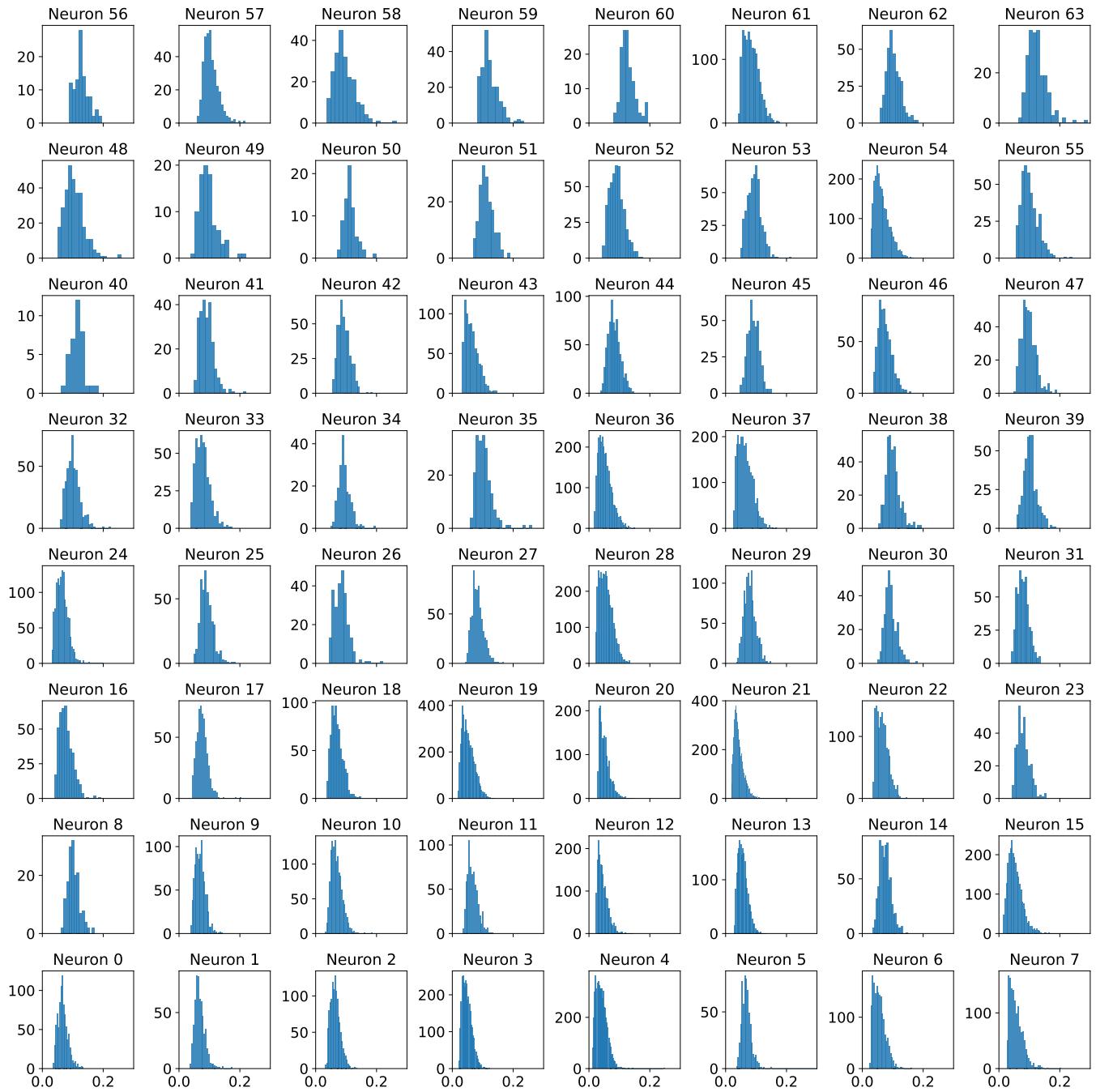


Figure 13. Intra-Neuron Distance distribution for the SOM used for spectral classification (see Figure 3). Neuron 0 is $z_{0,0}$, 1 is $z_{0,1}$, 8 is $z_{1,0}$, and so on.